Roche, O., et al., 2022, Long-runout pyroclastic density currents: Analysis and implications: Geology, v. 50, https://doi.org/10.1130/G50215.1

Long runout pyroclastic density currents: analysis and implications

Olivier Roche, Christopher D. Henry, Nourddine Azzaoui and Arnaud Guillin

Supplemental Material

We present supplementary Figs. S1-4 mentioned in the main text, detailed information on the Great Basin ignimbrites and the paleovalleys in which their parent PDCs flowed (Figs. S5-8), a summary of the database of Roche et al. (2021) presented in Table S2 and to which the Great Basin ignimbrites are compared, and the characteristics of the PDCs as well as the statistical model we use.

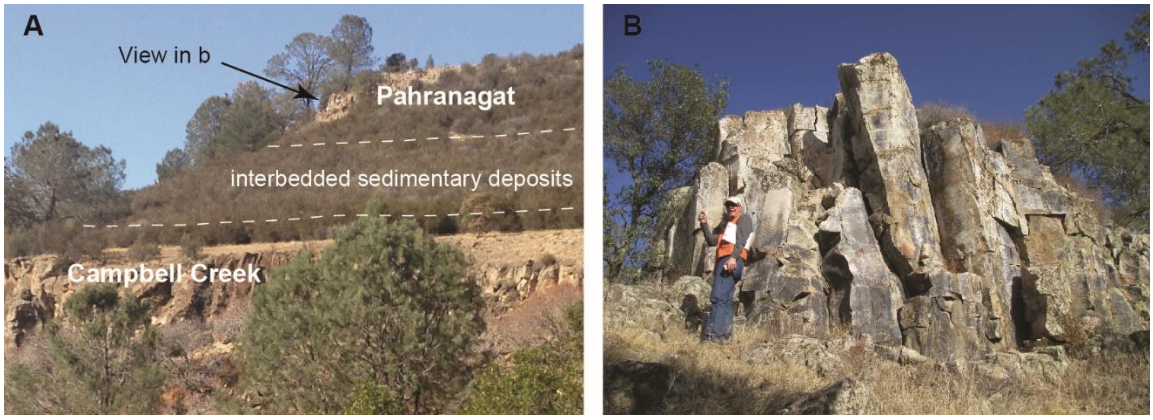

Fig. S1. Great Basin ignimbrites. (A) Outcrops of moderately welded 28.9 Ma Campbell Creek (lower ledge, 18 m thick) and 23.0 Ma Pahranagat (upper ledge, 15 m thick) ignimbrites at Valley Springs Peak, the western limit of their distribution (Fig. 1 in the main text). Approximate top of Campbell Creek and base of Pahranagat shown by the dashed lines; intervening deposit is poorly cemented gravel. Less welded tops of both ignimbrites are eroded, as are former deposits still farther west. (B) Moderately welded, columnar-jointed Pahranagat ignimbrite making upper ledge in (A).

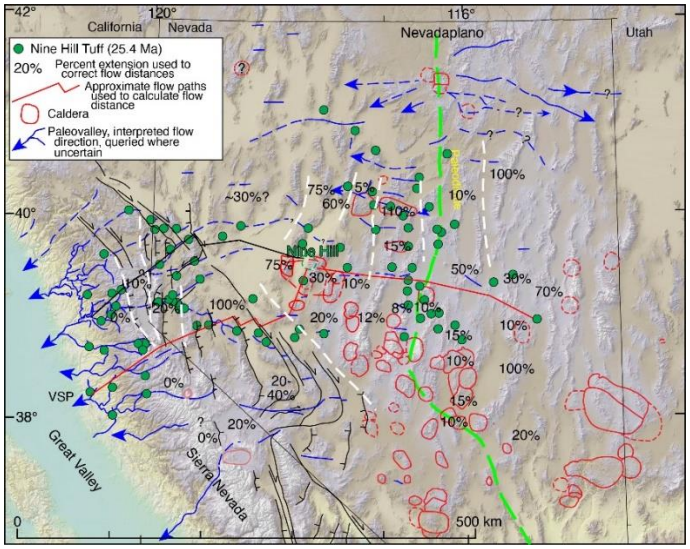

Fig. S2. Approximate flow paths and percent extension used to calculate flow lengths, including correction for post-depositional extension. Example of application to flow distance for the Nine Hill ignimbrite is given. See main text for sources of data.

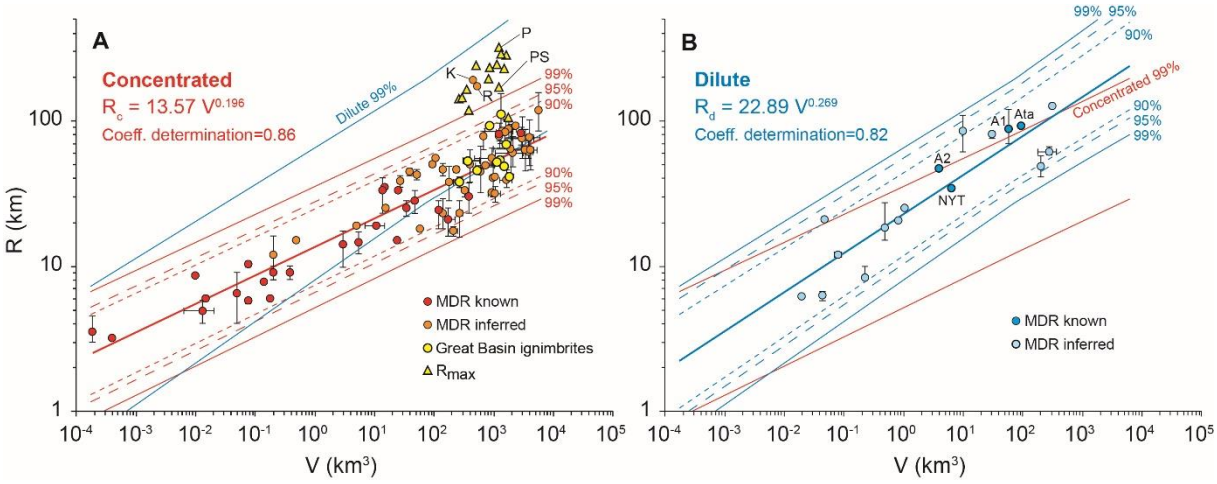

Fig. S3. Runout of PDCs, R, as function of bulk volume of outflow ignimbrite, V. (A) concentrated and (B) dilute parent currents with mass discharge rate (MDR) known from earlier studies or inferred from our analysis. For the Great Basin and the Peach Spring ignimbrites, R is the mean runout in directions sub-perpendicular to that of the maximum runout R_{max}. The power law relationships take into account all data except in (A) those of the Great Basin ignimbrites, Rattlesnake (Streck and Grunder, 1995) and Kidnappers (see below). Prediction intervals of 90, 95 and 99% are shown. Notation: (A) K: Kidnappers, P; Pahranagat, PS: Peach Spring, R: Rattlesnake; (B) A1: AsoI-1, A2: Aso 4I-2, NYT: Neapolitan Yellow Tuff.

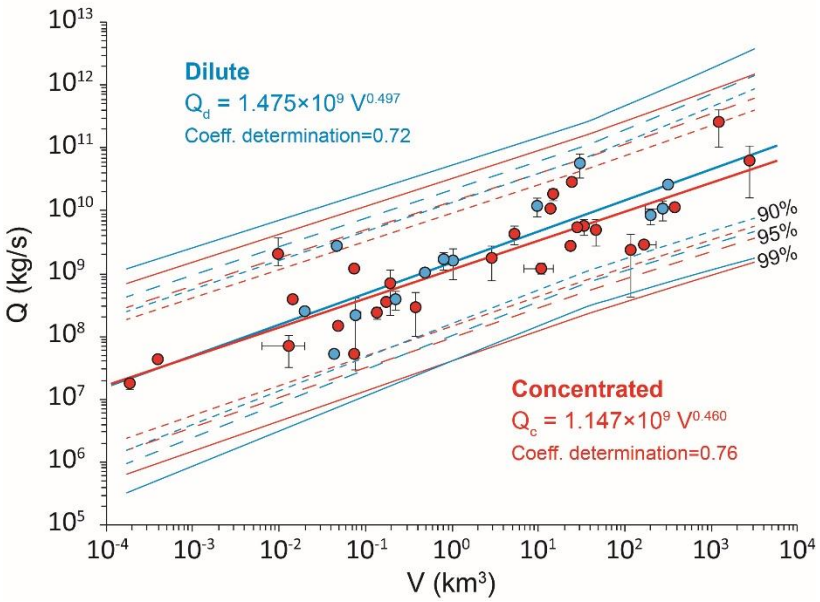

Fig. S4. Mass discharge rate, Q, as function of bulk volume of outflow ignimbrite, V. Data for concentrated or dilute parent PDCs from Roche et al. (2021; Table S2). Power law relationships and prediction intervals of 90, 95 and 99% are shown.

GREAT BASIN IGNIMBRITES

We present detailed information on the Great Basin ignimbrites and the paleovalleys in which their parent PDCs flowed. The distributions of the ignimbrites are shown in Figs. S5-8 and other properties are given in Table S1.

Correlation of the Great Basin ignimbrites

Ignimbrite correlation is based on stratigraphy, phenocryst assemblage, composition, remnant magnetic, and, most importantly, precise $^{40}Ar/^{39}Ar$ dates and K/Ca of dated sanidines, which is a very useful secondary correlation tool (Henry, 2008; Hinz et al., 2009; Henry and Faulds, 2010; Henry et al., 2012). Only a few ignimbrites are compositionally or petrographically distinctive. Almost all are rhyolites, with approximately equal numbers of sparsely porphyritic (≤15% phenocrysts) and abundantly porphyritic (~20–50% phenocrysts) units (Henry and John, 2013). Both sparsely and abundantly porphyritic rhyolites commonly show compositional or petrographic evidence of zoning to trachydacites or dacites. All contain variable proportions of sanidine, plagioclase, quartz, and biotite, and less silicic units or zones contain minor hornblende and/or clinopyroxene. The considerable overlap in phenocryst assemblage and composition makes these poor discriminators. Distinctive units include the sparsely porphyritic Nine Hill ignimbrite, which contains three feldspars (sanidine, anorthoclase, and plagioclase), has high Zr and Nb contents (~400 and 30 ppm, respectively), and is zoned from ~77% to 68% SiO_2 (Deino, 1985; Henry and John, 2013). Nine Hill sanidines also have distinctive low K/Ca of ~10-12, whereas most Great Basin ignimbrites have K/Ca of ~30 to 100 (Henry and Faulds, 2010).

Correction of flow distances for extension

Flow distances were corrected for spatially variable extension in the Basin and Range Province (Fig. 1 in the main text; Fig. S2). Major extension in the Great Basin began ~16-17 Ma and post-dates all the ignimbrites discussed here (Colgan and Henry, 2009). The caldera belt is the least extended part of the Great Basin because the plutonic region that fed and underlies the belt resisted major extension (Long, 2019). Areas at the edge of and outside the caldera belt locally underwent as much as 100% extension (e.g., Colgan et al., 2008). In addition to the preceding references, we use published geologic maps and regional estimates of extension (Henry and Faulds, 2010; Cassel et al., 2012) to correct present-day distances. The Sierra Nevada was not extended, so present-day distances require no correction. Our corrections assume that paleovalleys are linear and down the Sierra Nevada topographic gradient, which is an oversimplification at either large or small scale (Lindgren, 1911; Cassel and Graham, 2011; Fig. 1 in the main text, Figs. S5-8). True flow distances would be greater than our estimates but require too many assumptions to be reliable.

Recognition and mapping of paleovalleys

Paleovalleys in which the PDCs flowed and were deposited are generally much wider (8-10 km) than deep (≤1 km), in relatively easily erodible rocks, predominantly Mesozoic granitoids that were weathered and eroded during the warm, wet Eocene climate (Henry and Fauld, 2010; Henry et al., 2012; Henry and John, 2013; Mudelsee et al., 2014; Christensen et al., 2015; see Fig. 1 in the main text). Paleovalleys are locally much narrower (1-2 km) in highly resistant, metamorphic rocks. Geologists mapped the paleovalleys in great detail in the Sierra Nevada in the late 1800s and early 1900s because Eocene gravels that occupy bottoms of paleovalleys contained considerable gold (Lindgren, 1911; Yeend, 1974; Christensen et al., 2015). This old work connected major gold-bearing gravel deposits but whether these connected the same channel, different channels, or meanders in one wider, braided channel is not always certain (Yeend, 1974; Cassel and Graham, 2011). Paleovalleys in the Sierra Nevada were generally grouped into west-southwest segments, down the topographic gradient, and north-northwest segments that aligned with major structural-lithologic boundaries (Lindgren, 1911). Although workers in the Sierra Nevada recognized that the paleovalleys had headwaters east of the present Sierra Nevada crest (Bateman and Wahrhaftig, 1966; Yeend, 1974), continuation of the paleovalleys into the Great Basin was only recognized beginning about 2000 (Davis et al., 2000; Henry

et al., 2003; Garside et al., 2005). Identification and mapping of paleovalleys in the Basin and Range varies from detailed (e.g., Henry et al., 2004; Henry et al., 2009; Henry and Faulds, 2010) to reconnaissance (Henry et al., 2012; Henry, 2008) to not at all (Figs. S5-8). Paleovalleys are broadly mapped across the northern Great Basin, whereas only minor segments are recognized in the southern part. Individual ignimbrites in paleovalleys are incompletely preserved-exposed because of shortly post-emplacement and later, late Cenozoic – Quaternary erosion, and covered by younger rocks in the unfaulted Sierra Nevada. The same factors affected ignimbrites in the highly faulted and extended Great Basin, especially cover in large basins.

Evidence that ignimbrites primarily flowed and were deposited in paleovalleys

That ignimbrites primarily flowed in paleovalleys is demonstrated by their preservation almost entirely in the deepest parts of paleovalleys, both in the Great Basin and the Sierra Nevada, where they are interbedded with fluvial deposits and wedge out against paleovalley walls composed of Mesozoic or Paleozoic rocks (Fig. 1B in the main text). Ignimbrites of any kind are generally not preserved over the mostly flat interfluves. Thin, interfluve-veneering deposits from the dilute parts of two-layer PDCs may have been deposited but were rapidly eroded. Distal and partly stratified deposits of this type are only preserved for Nine Hill, which had magmatic temperature up to 950°C (Deino, 1985), and Campbell Creek; these two units are commonly welded even where only a few meters thick. Any veneering deposits from the dilute part of cooler PDCs would have been poorly or non-welded and probably rapidly eroded. In the northern Great Basin, where paleovalleys and their contained ignimbrites are best mapped, most ignimbrites demonstrably were channelized into one or two paleovalleys and are therefore only found in those paleovalleys in the Sierra Nevada (e.g., Axehandle and Rattlesnake; Figs. S5-8). Ignimbrites farther south (e.g., Pahranagat, Fig. 1A in the main text) flowed as far west in the Sierra Nevada as those to the north, but lesser detailed mapping hampers determining specific paleovalleys and flow paths.

The variation in mapping detail bears on total flow distances and whether some Great Basin ignimbrites have non-elliptical distributions. For example, Best et al. (2013b) recognized Underdown (their Clipper Gap), Pahranagat, and Windous only east of or <50 km west of their respective calderas (Fig. 1A in the main text; Figs. S5 and S8). This more limited work underestimates total flow distances and suggests highly asymmetric distributions. Our new work (this report; Henry, unpublished data; see also Lee et al., 2020) demonstrates that all three parent PDCs flowed far to the west to the western foothills of the Sierra Nevada. Without the new data and corrected for extension, these ignimbrites would appear to have a more circular distribution that is highly asymmetric to source calderas. Extensive eastward flow of each of these units is consistent with their emplacement on a high plateau with a gentle paleodivide and significant relief was restricted to paleovalleys (Henry and John, 2013). The apparent restriction of the tuff of Toiyabe to west of its caldera likely also reflects insufficient mapping to the east (Fig. S8).

The presence of the Rattlesnake Canyon ignimbrite in a paleovalley south of its main distribution raises the possibility of avulsion in the western, lower elevation parts of paleovalleys (Fig. S5). Rattlesnake Canyon and the slightly older Axehandle ignimbrite are preserved mostly in a single, northern paleovalley, but Rattlesnake Canyon is also found in the lower reaches of the next major drainage to the south, where it occurs ~200 m below its outcrops to the north. This southern presence could indicate flow in both paleovalleys, and non-preservation or recognition in the upper part of the southern valley, or avulsion from the northern into the southern in the westernmost part where interfluves locally were at ≤100 m above the channel.

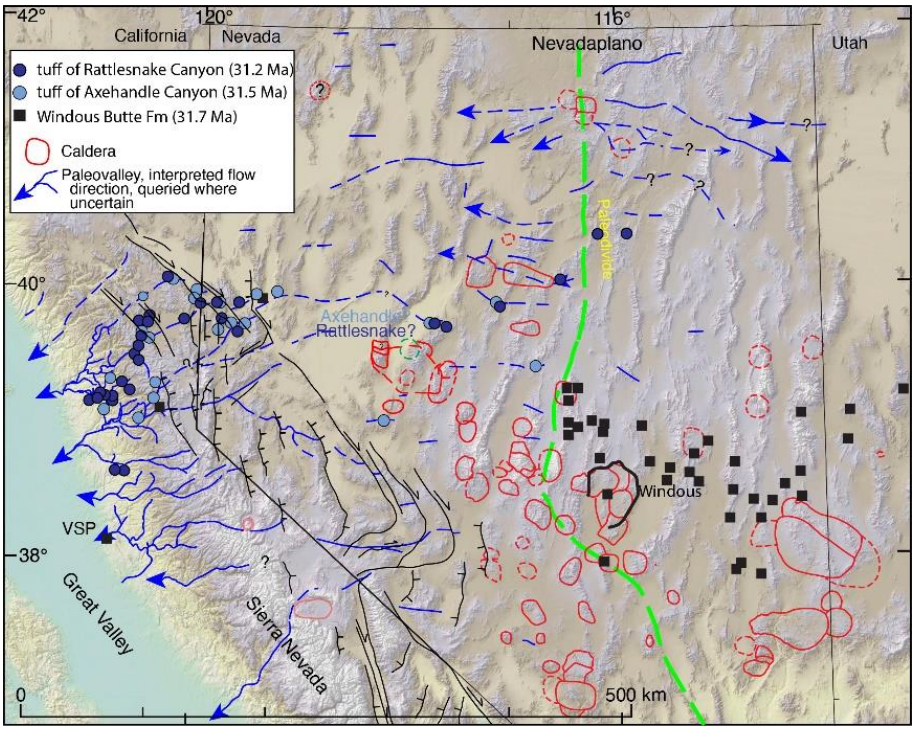

Fig. S5. Great basin ignimbrites. Distributions and source calderas of 31.7 Ma Windous Butte, 31.5 Ma Axehandle Canyon, and 31.2 Ma Rattlesnake Canyon ignimbrites. Source calderas of Axehandle and Rattlesnake Canyon are buried, probably in the area shown.

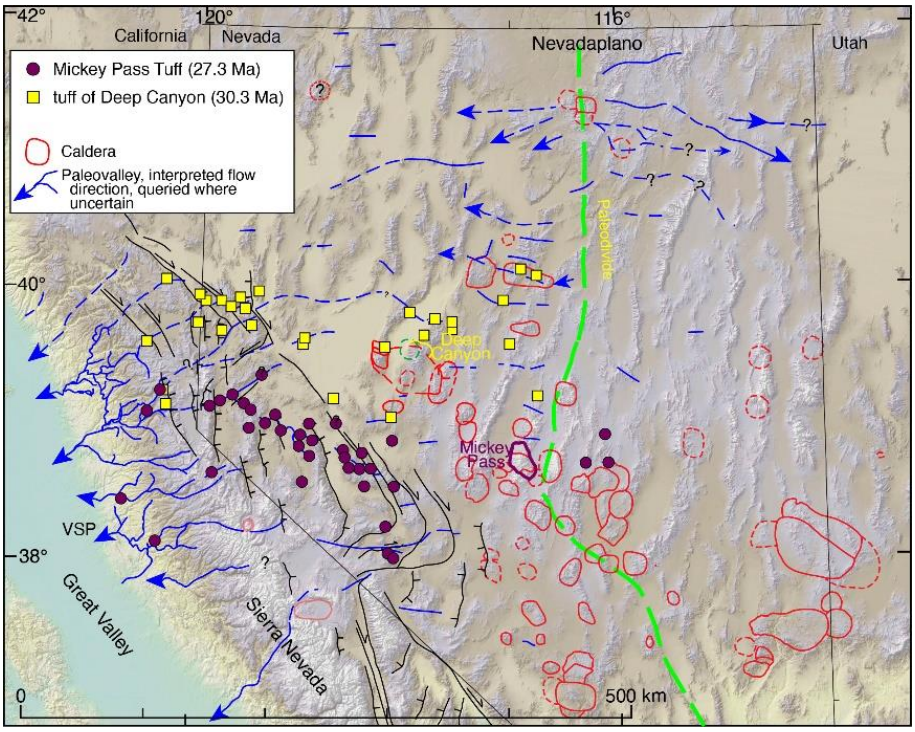

Fig. S6. Great basin ignimbrites. Distributions and source calderas of 30.3 Ma Deep Canyon and 27.3 Ma Mickey Pass ignimbrites.

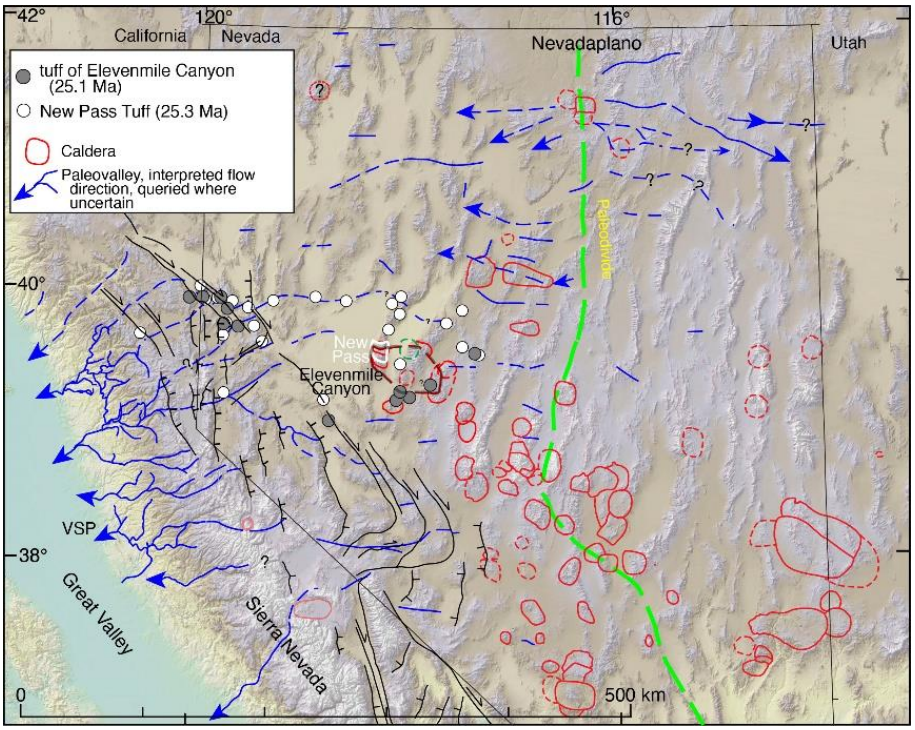

170
171
172 **Fig. S7.** Great basin ignimbrites. Distributions and source calderas of 25.3 Ma New Pass and 25.1 Elevenmile
173 Canyon ignimbrites.
174
175

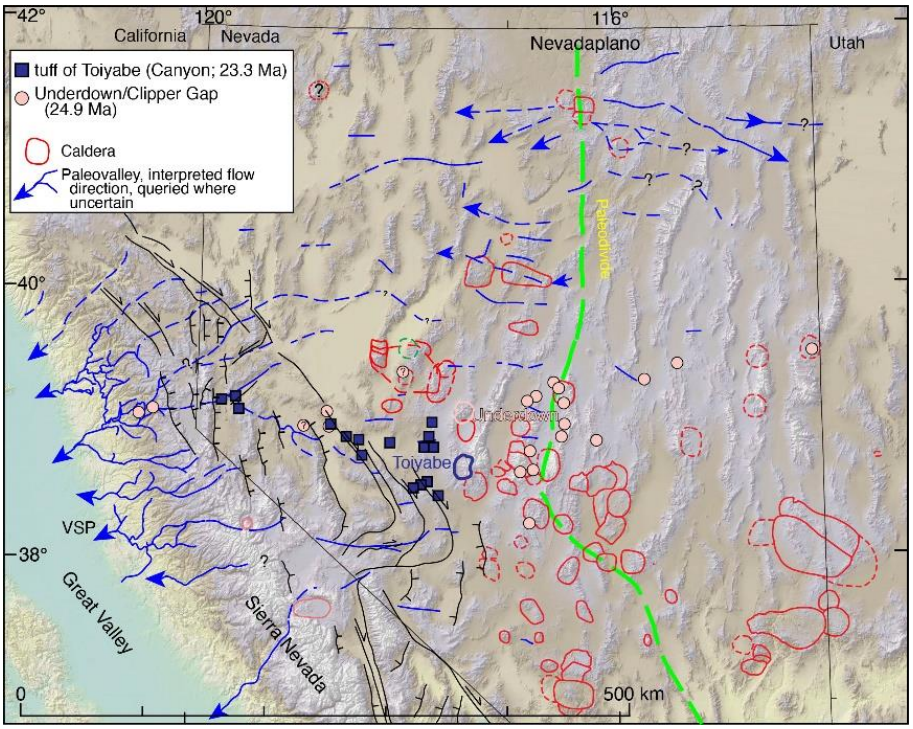

176
177
178 **Fig. S8.** Great basin ignimbrites. Distributions and source calderas of 24.9 Ma Underdown and 23.3 Ma Toiyabe
179 ignimbrites.
180
181

DATABASE

Table S2 presents the database of Roche et al. (2021) but neglecting Oruanui, whose volume estimates are only orders of magnitude (Wilson, 2001), and considering additional cases: Aso 4I-3 and 4II-3 (Kaneko et al., 2007), Atana and Toconao (Lindsay et al., 2001a,b), Cerro Panizos (Ort, 1993), Loma Seca units S and V (Hildreth at al., 1984), Toya, unit 2c (Ito, 2014; Goto et al., 2018). Almost all of the Great Basin ignimbrites that appear to have more circular distributions were generated by eruptions from calderas east of the paleodivide of Fig. 1 in the main text (Best et al., 2013a and 2013b). Their circular distributions may be real and reflect mostly eastward flow to a base level of intracontinental basins that were well above sea level. Alternatively, these ignimbrites may correlate to those farther west, but confirmation will require additional mapping and precise dating.

CHARACTERISTICS OF PYROCLASTIC DENSITY CURRENTS

We compare new data from 12 eruptions in the Great Basin ignimbrite province (Table S1), most of which PDCs traveled unusually long distances, to the database of Roche et al. (2021, Table S2). Following this reference, we first consider the types of PDCs (i.e., dilute or concentrated) based on the sedimentological characteristics and architecture of ignimbrites described by the authors and on the ignimbrites aspect ratios. We recognize that this approach has limitations but the types of PDCs can be confirmed in a second step by considering the relationship between the runout and the mass discharge rate (Fig. 4 in the main text). The Great Basin ignimbrites have aspect ratios greater than $\sim 5\times10^{-5}$ indicating two-layer parent currents with a concentrated base consistent with other ignimbrites features (Fig. 2 in the main text).

The two essential parameters for our study are the runout distance of the PDCs and the eruption mass discharge rate (MDR). We determine the runout by taking into account the asymmetry of the areal extent of ignimbrites around their respective eruptive sources (see limitations to estimating runout distance in Roche et al., 2021). For this purpose, we define the ratio R_{max}/R, with R_{max} the maximum runout and R the mean runout in two, or alternatively one, directions sub-perpendicular to that of R_{max} (Fig. 3A in the main text). The MDRs for several eruptions in the database of Roche et al. (2021), and those of the Great Basin province, are unknown. Accordingly, we infer these MDRs from the power law relationship given by Roche et al. (2021; their Fig. 8b) between the bulk volume of outflow ignimbrites and the known MDRs for eruptions that produced 28 concentrated and 14 dilute PDCs. However, for concentrated PDCs, we exclude Kidnappers (Wilson et al., 1995) and Rattlesnake (Streck and Grunder, 1995) for the following reasons. The MDR estimates for these two eruptions are from a dilute PDC model (Dade, 2003) and it appears that the good agreement of these data with the power law relationship between runout and MDR given by Roche et al. (2021; their Fig. 4) is probably a coincidence. Furthermore, when considering the relationship between PDC runout and ignimbrite volume, the data for Kidnappers and Rattlesnake are clearly outside the prediction intervals for concentrated currents (Fig. S3). Excluding these two cases, we obtain for the concentrated PDCs the following power law relationship between mass discharge rate, Q, and volume, V,

$$Q=1.147\times10^{9}\times V^{0.460} \quad (1)$$

(Fig. S4), which is nevertheless very close to that of Roche et al. (2021; $Q=1.412\times10^{9}\times V^{0.537}$). Interestingly, this relationship is also very close to that for dilute PDCs, $Q_d=1.475\times10^{9}\times V^{0.497}$, implying that the MDR estimates we give vary little with the type of PDC assigned.

In the context described above, determining the bulk volumes of the Great Basin ignimbrites is an important step for our analysis but is not straightforward. In fact, estimating volumes from ignimbrites average thicknesses and areas is elusive because the former often vary from a few meters in unconfined areas to >200-300 m in some valleys (even in distal domains >100 km from the source; Henry and Faulds, 2010) and depends also on possible compaction related to welding while the latter may be overestimated (see main text). Although an error as large as one order of magnitude, for example, would not affect the conclusions of our study, we prefer to estimate the bulk volume of the ignimbrites in another way. We first calculate the total dense rock equivalent volume of each eruption ($V_{t,DRE}$) from the caldera area and the subsidence depth, which are generally well constrained. Then, we convert $V_{t,DRE}$ to outflow ignimbrite bulk volume from the average ratio $V/V_{t,DRE}\sim0.6$ according to the database of

Roche et al. (2021). Estimates of bulk volumes of the Great Basin ignimbrites are given in Table S1. In three cases where calderas are buried (Axehandle, Nine Hill, Rattlesnake Canyon), we nevertheless calculate the volume by considering the ignimbrite area and an average thickness of 25 m, typical of the other Great Basin ignimbrites, which leads to overestimates.

Statistical model to infer eruption mass discharge rate

We use the statistical link between volume and MDR (Equation 1) to determine the missing MDR values. In this case, the runout prediction intervals are influenced by both the MDR's fit uncertainty

$$R = \mu_2 + Q\,\beta + \varepsilon_2 \qquad (2)$$

and the uncertainty of predicting the missing MDR from the volume

$$Q = \mu_1 + V\,\gamma + \varepsilon_1. \qquad (3)$$

In this model, the parameters are fitted using the observed volumes and MDRs. The non-observed MDRs are then imputed using observed volumes from equation (3). The errors ε_1 and ε_2 are independent with zero mean and have variances σ_1 and σ_2; the parameters μ_1, μ_2, γ and β are estimated via a penalized least squares procedure (see for instance Hastie et al., 2009). We denote $\widehat{S_1}$ and $\widehat{S_2}$, respectively, the residual estimated standard deviations of equations (2) and (3). The methodology for calculating the prediction intervals is the following. We define, for a risk α_1, the interval $I = [m, M]$ giving the prediction interval of the MDR from equation (3). In this case, $m = \widehat{\mu_1} + V\hat{\gamma} - t_{1-\alpha_1}\,\widehat{S_1}$ and $M = \widehat{\mu_2} + V\hat{\beta} + t_{1-\alpha_1}\,\widehat{S_1}$. The term $t_{1-\alpha_1}$ is a corrected quantile corresponding to 1-α_1 of the student distribution. Since the estimated slope coefficient β is positive, we deduce the final prediction interval of the runout $I = [m - t_{1-\alpha_2}\,\widehat{S_2}; M + t_{1-\alpha_2}\,\widehat{S_2}]$. This technique is an adaptation of meta-models procedures (Friedrich and Knapp, 2013). The choice of the risks α_1 and α_2 is made so that the final risk of the interval I is equal to a desired risk α. In Fig. 4 in the main text, the prediction intervals are given for α=0.90, 0.95 and 0.99.

REFERENCES CITED

Bateman, P.C. and Wahrhaftig, C., 1966, Geology of the Sierra Nevada, in Bailey, E.H., ed., Geology of northern California: California Division of Mines and Geology Bulletin 190, p. 107–172.

Best, M.G., Christiansen, E.H., Deino, A.L., Gromme, S., Hart, G.L., and Tingey, D.G., 2013, The 36–18 Ma Indian Peak–Caliente ignimbrite field and calderas, southeastern Great Basin, USA: Multicyclic super-eruptions: Geosphere, v. 9, no. 4, p. 964-950, doi:910.1130/GES00902.00901.

Best, M.G., Gromme, S., Deino, A.L., Christiansen, E.H., Hart, G.L. and Tingey, D.G., 2013b, The 36–18 Ma Central Nevada ignimbrite field and calderas, Great Basin, USA: Multicyclic super-eruptions: Geosphere, v. 9, p. 1562-1636, doi:1510.1130/GES00945.00941.

Cassel, E.J. and Graham, S.A., 2011, Paleovalley morphology and fluvial system evolution of Eocene–Oligocene sediments ("auriferous gravels"), northern Sierra Nevada, California: Implications for climate, tectonics, and topography: Geological Society of America Bulletin, v. 123, no. 9–10, p. 1699–1719, doi:10.1130/B30356.1.

Cassel, E.J., Graham, S.A., Chamberlain, C.P. and Henry, C.D., 2012, Early Cenozoic topography, morphology, and tectonics of the northern Sierra Nevada and western Basin and Range: Geosphere, v. 8, p. 229-249, https://doi.org/10.1130/GES00671.1.

Christensen, O.D., Henry, C.D., and Wood, J., 2015, Origin of gold in placer deposits of the Sierra Nevada foothills, California: Geological Society of Nevada, New Concepts and Discoveries, W.M. Pennell and L.J. Garside, eds., 2015 Symposium Volume, Reno/Sparks, Nevada, p. 833-859.

Colgan, J.P. and Henry, C.D., 2009, Rapid middle Miocene collapse of the Sevier orogenic plateau in north-central Nevada: International Geology Review, v. 51, p. 920-961, https://doi.org/10.1080/00206810903056731.

Colgan, J.P., John, D.A., Henry, C.D. and Fleck, R.J., 2008, Large-magnitude Miocene extension of the Eocene Caetano caldera, Shoshone and Toiyabe Ranges, Nevada: Geosphere, v. 4, p. 107-131, doi:10.1130/GES00115.1.

Dade, W.D., 2003, The emplacement of low-aspect ratio ignimbrites by turbulent parent flows: Journal of Geophysical Research, v. 108, 2211.

Davis, D.A., Henry, C.D., Garside, L.J., Faulds, J.E., and Goldstrand, P.M., 2000, Eocene-Oligocene paleovalleys cross the Sierra Nevada – Basin and Range boundary, western Nevada and eastern California: Geological Society of America Abstracts with Programs, v. 32, no. 7, p. A-167.

Deino, A.L., 1985, Stratigraphy, chemistry, K-Ar dating, and paleomagnetism of the Nine Hill Tuff, California-Nevada: Part I. Unpub. Ph.D. thesis. Berkeley, University of California, 338 p.

Friedrich, T. and Knapp, G., 2013, Generalised interval estimation in the random effects meta regression model: Computational Statistics & Data Analysis, v. 64, p. 165-179, https://doi.org/10.1016/j.csda.2013.03.011.

Garside, L.J., Henry, C.D., Faulds, J.E., and Hinz, N.H., 2005, The upper reaches of the Sierra Nevada auriferous gold channels, in Rhoden, H.N., et al., eds., Window to the World, Geological Society of Nevada Symposium Proceedings, May 14-18, 2005, p. 209-235.

Goto, Y., Suzuki, K., Shinya, T., Yamauchi, A., Miyoshi, M., Danhara, T., and Tomiya, A., 2018, Stratigraphy and lithofacies of the Toya ignimbrite in southwestern Hokkaido, Japan: Insights into the caldera-forming eruption at Toya Caldera: Journal of Geography (Chigaku Zasshi）, v. 127, no. 2, p. 191-227, doi:10.5026/jgeography.127.191

Hastie, T., Tibshirani, R. & Friedman, J., 2009, The elements of statistical learning. Data mining, inference, and prediction. Second edition (Springer Series in Statistics). Springer, New York.

Henry, C.D., 2008, Ash-flow tuffs and paleovalleys in northeastern Nevada: Implications for Eocene paleogeography and extension in the Sevier hinterland, northern Great Basin: Geosphere, v. 4, p. 1-35, doi:10.1130/GES00122.1.

Henry, C.D., Faulds, J.E., dePolo, C.M., and Davis, D.A., 2004, Geology of the Dogskin Mountain Quadrangle, northern Walker Lane, Nevada: Nevada Bureau of Mines and Geology Map 148, scale 1:24,000, 13 p. text.

Henry, C. D. & Faulds, J. E., 2010, Ash-flow tuffs in the Nine Hill, Nevada, paleovalley and implications for tectonism and volcanism of the western Great Basin, USA: Geosphere, v. 6, p. 339-369, doi:310.1130/GES00548.00541.

Henry, C.D., Faulds, J.E., Garside, L.G., and Hinz, N.H., 2003, Tectonic implications of ash-flow tuffs in paleovalleys in the western US: Geological Society of America Abstracts with Programs, v. 35, no. 6, p. 346.

Henry, C.D., Hinz, N.H., Faulds, J.E., Colgan, J.P., John, D.A., Brooks, E.R., Cassel, E.J., Garside, L.J., Davis, D.A., and Castor, S.B., 2012, Eocene–Early Miocene paleotopography of the Sierra Nevada–Great Basin–Nevadaplano based on widespread ash-flow tuffs and paleovalleys: Geosphere, v. 8, no. 1, p. 1-27, doi:10.1130/GES00727.00721.

Henry, C. D. and John, D. A., 2013, Magmatism, ash-flow tuffs, and calderas of the ignimbrite flareup in the western Nevada volcanic field, Great Basin, USA: Geosphere, v. 9, p. 951-1008, doi:1010.1130/GES00867.00861.

Henry, C.D., Ramelli, A.R., and Faulds, J.E., 2009, Geologic map of the Seven Lakes Mountain Quadrangle, Washoe County, Nevada and the eastern part of the Constantia Quadrangle, Lassen County, California: Nevada Bureau of Mines and Geology Map 164, 1:24,000, 27 p. text.

Hildreth, W., Grunder, A.L. and Drake, R.E., 1984, The Loma Seca Tuff and the Calabozos caldera: A major ash-flow and caldera complex in the southern Andes of central Chile: Geological Society of America Bulletin, v. 95, p. 45-54.

Hinz, N.H., Faulds, J.E. and Henry, C.D., 2009, Tertiary volcanic stratigraphy and paleotopography of the Diamond and Fort Sage Mountains, northeastern California and western Nevada–Implications for development of the northern Walker Lane, in Oldow, J.S. & Cashman, P.H., eds., Late Cenozoic structure and evolution of the Great Basin–Sierra Nevada transition: Geological Society of America Special Papers, v. 447, p. 101-132, doi:10.1130/2009.2447(07).

Ito, H., 2014, Zircon U–Th–Pb dating using LA-ICP-MS: Simultaneous U–Pb and U–Th dating on the 0.1 Ma Toya Tephra, Japan: Journal of Volcanology and Geothermal Research, v. 289, p. 210-223, http://dx.doi.org/10.1016/j.jvolgeores.2014.11.002.

Kaneko, K., Kamata, H., Koyaguchi, T., Yoshikawa, M. and Furukawa, K., 2007, Repeated large-scale eruptions from a single compositionally stratified magma chamber: An example from Aso volcano, Southwest Japan. Journal of Volcanology and Geothermal Research, v. 167, p. 160-180, doi:110.1016/j.jvolgeores.2007.1005.1002.

Lee, J., Hoxey, A.K.R., Calvert, A., and Dubyoski, P., 2020, Plate boundary trench retreat and dextral shear drive intracontinental fault-slip histories: Neogene dextral faulting across the Gabbs Valley and Gillis Ranges, central Walker Lane, Nevada: Geosphere, v. 16, p. 1249-1275, https://doi.org/10.1130/GES02240.1.

Lindgren, W., 1911. The Tertiary gravels of the Sierra Nevada of California: US Geological Survey Professional Paper, v. 73, 226 pages.

Lindsay, J.M., de Silva, S., Trumbull, R., Emmermann, R. and Wemmer, K., 2001a, La Pacana caldera, N. Chile: a re-evaluation of the stratigraphy and volcanology of one of the world's largest resurgent calderas: Journal of Volcanology and Geothermal Research, v. 106, p. 145-173.

Lindsay, J.M., Schmitt, A.K., Trumbull, R.B., De Silva, S.L., Siebel, W., and Emmermann, R., 2001, Magmatic evolution of the La Pacana caldera system, central Andes, Chile: Compositional variation of two cogenetic, large-volume felsic ignimbrites: Journal of Petrology, v. 42, no. 3, p. 459-486.

Long, S.P., 2019, Geometry and magnitude of extension in the Basin and Range Province (39°N), Utah, Nevada, and California, USA: Constraints from a province-scale cross section: Geological Society of America Bulletin, v. 131, no. 1-2, p99-119, https://doi.org/10.1130/B31974.1.

Mudelsee, M., Bickert, T., Lear, C.H., Lohmann, G., 2014, Cenozoic climate changes: A review based on time series analysis of marine benthic δ18O records: Reviews of Geophysics, v. 52, p. 333-374, https://doi.org/10.1002/2013RG000440.

Ort, M.H., 1993, Eruptive processes and caldera formation in a nested downsag collapse caldera: Cerro Panizos, central Andes Mountains: Journal of Volcanology and Geothermal Research, v. 56, p. 221-252.

Roche, O., Azzaoui, N. and Guillin, A., 2021, Discharge rate of explosive volcanic eruption controls runout distance of pyroclastic density currents: Earth and Planetary Science Letters, v. 568, 117017, https://doi.org/10.1016/j.epsl.2021.117017.

Streck, M.J. and Grunder, A.L. Crystallization and welding variations in a widespread ignimbrite sheet; the Rattlesnake Tuff, eastern Oregon, USA: Bulletin of Volcanology, v. 57, p. 151-169.

Wilson, C.J.N., 2001, The 26.5 ka Oruanui eruption, New Zealand: an introduction and overview: Journal of Volcanology and Geothermal Research, v. 112, p. 133-174.

Wilson, C.J.N., Houghton, B.F., Kamp, P.J.J. and McWilliams, M.O., 1995, An exceptionally widespread ignimbrite with implications for pyroclastic flow emplacement: Nature, v. 378, p. 605-607.

Yeend, W.E., 1974, Ancestral Yuba River, Sierra Nevada, California: United States Geological Survey Professional Paper, v. 772, 44 pages.

Supplementary Table 1. Properties of the elliptical Great Basin and Peach Spring ignimbrites.

Ignimbrite/tuff (other name)	**Age (Ma)**	**Runout distance (km)**				**R (km)**	**R_{max}/R**	**$V_{t,DRE}$ (km^3)**	**V (km^3)**	**A (km^2)** [a]	**H (m)** [a]	**AR**	**Q (kg/s)** [b]	**Q range (kg/s)** [b]
		West	South	East	North									
Axehandle Canyon [c]	31.5	**238**	53	66	38	45.5	5.2		520 [e]	21000		1.5E-04	2.0E+10	0.9-4.5E+10
Campbell Creek [d]	28.9	**228**		217	49	49	4.7	2500	1500	55000	27	1.0E-04	3.3E+10	1.4-8.0E+10
Deep Canyon (Cove spring) [e]	30.4	**165**	53	82		53	3.1	600	360	24000	15	8.6E-05	1.7E+10	0.8-3.7E+10
Elevenmile Canyon	25.1	**105**	41	26		41	2.6	3000	1800				3.6E+10	1.5-8.9E+10
Mickey Pass (Mt Jefferson) [f]	27.3	**244**		52		52	4.7 [k]	1900	1140	24000		2.7E-04	2.9E+10	1.3-6.9E+10
New Pass (Chimney spring, Poco canyon) [g]	25.3	**142**	41	56	35	38	3.7	450	270	10000	27	2.4E-04	1.5E+10	0.7-3.1E+10
Nine Hill [h]	25.4	**285**	69	202	152	111	2.6		1337 [l]	54000		9.4E-05	3.2E+10	1.3-7.5E+10
Pahranagat	23.0	**314**	54	109	54	54	5.8	2100	1260	40000	32	1.4E-04	3.1E+10	1.3-7.3E+10
Rattlesnake Canyon [i]	31.2	**230**		130		130			867 [l]	35000		1.2E-04	2.6E+10	1.1-5.9E+10
Toiyabe (Santiago canyon)	23.3	**144**						500	300				1.6E+10	0.8-3.3E+10
Underdown (Clipper gap)	24.9	**192**	93	190		93	2.1	1400	840	38000	22	1.0E-04	2.5E+10	1.1-5.8E+10
Windous Butte [j]	31.7	**280**		144	69	69	4.1	2700	1620	63000	26	9.1E-05	3.4E+10	1.4-8.4E+10
Peach Spring [m]	18.8	**170**	97	101	64	81	2.1	640	1231	32000	38	1.9E-04	2.4E+11	1.0-3.8E+11

Notation. R: mean runout in directions sub-perpendicular to the maximum runout R_{max}, $V_{t,DRE}$: total dense rock equivalent volume of eruption, V: bulk volume of outflow ignimbrite, A: area, H: mean thickness, AR: aspect ratio, Q: eruption mass discharge rate.

[a] Conservative estimates. [b] Estimated from V_{bulk} (except Peach Spring), ranges are 95% confidence inrervals. [c] Caldera buried. [d] Minimum volume estimates. [e] $V_{t,DRE}$ ±260 km^3 (Henry, C. D. & John, D. A., 2013, Magmatism, ash-flow tuffs, and calderas of the ignimbrite flareup in the western Nevada volcanic field, Great Basin, USA. *Geosphere* 9, 951-1008, doi: 1010.1130/GES00867.00861). [f] Minimum volume estimates. [g] Caldera highly extended. [h] Caldera partly buried. [i] Caldera buried. Not to be confused with Rattlesnake tuff (Streck, M. J. & Grunder, A. L., 1995, Crystallization and welding variations in a widespread ignimbrite sheet; the Rattlesnake Tuff, eastern Oregon, USA. *Bull. Volcanol.* **57**, 151-169). [j] $V_{t,DRE}$ ±500 km^3. [k] R considered in east direction. [l] Assuming a typical mean thickness of 25 m for the Great Basin ignimbrites. [m] Roche, O., Buesch, D. C. & Valentine, G. A., 2016, Slow-moving and far-travelled dense pyroclastic flows during the Peach Spring super-eruption. *Nat. Commun.* **7**, 10890, doi: 10810.11038/ncomms10890.